Table 1
Fold-changes of expression of "chemokine genes" after rhAIF-stimulation of isolated $CD14^+$ PBMCs. Signals and ratios were determined according to Affymetrix algorithms and procedures.

Probe set ID	AIF signal	NC signal	Ratio	Gene title
206365_at	499.7	27.9	13.00	CCL-1
216598_s_at	1325.1	237.0	4.00	CCL-2
205114_s_at	47689.5	5122.8	9.19	CCL-3
204103_at	48797.1	6007.6	8.00	CCL-4
1405_i_at	130.7	9.8	9.85	CCL-5
208075_s_at	195.1	69.5	2.00	CCL-7
214038_at	753.5	283.7	3.48	CCL-8
210133_at	26.5	54.8	0.57	CCL-11
216714_at	213.7	105.2	2.14	CCL-13
210390_s_at	3128.5	110.2	25.99	CCL-14, CCL-15
207354_at	122.5	56.5	2.64	CCL-16
207900_at	37.2	40.1	0.71	CCL-17
32128_at	888.7	334.4	2.14	CCL-18
210072_at	237.2	384.1	1.15	CCL-19
205476_at	7638.8	67.7	45.25	CCL-20
204606_at	92.6	416.7	0.22	CCL-21
207861_at	153.0	124.2	1.23	CCL-22
210548_at	580.0	28.5	16.00	CCL-23
221463_at	5081.6	694.9	6.50	CCL-24
206988_at	104.1	41.2	1.74	CCL-25
223710_at	64.2	128.2	0.38	CCL-26
230327_at	211.9	213.4	1.32	CCL-27
224240_s_at	358.6	629.9	0.93	CCL-28

T cells that secrete AIF-1 upregulate the proliferation of VSMCs [12]. Moreover, LPS-stimulated macrophages expressed AIF-1 and secreted interleukin IL-6, IL-10 and IL-12p40 [13]. Thus, *AIF-1* gene expression is involved in specific inflammatory signaling pathways related to T cell activation. Moreover, rhAIF itself can induce chemotaxis and proliferation as well as IL-6 production in synovial fibroblasts from patients with RA and in normal human fibroblasts [7,8]. IL-6 and AIF-1 concentrations in synovial fluid were significantly elevated in patients with RA compared with patients with osteoarthritis. There was a positive correlation between the synovial fluid levels of AIF-1 and IL-6. In this study of $CD14^+$ PBMCs, rhAIF-1 induced expression of chemokine-related genes and enhanced secretion of CCL3/MIP-1α, together with IL-6 and small amounts of other chemokines. It is reported that CCL3/MIP-1α induced chemotaxis in monocytic cells by more than 1 ng/mL [14]. Actually, we applied CCL3/MIP-1α as reference control at 0.5, 5, 50, 150 ng/mL in PBMC migration, but the chemotaxis was induced at a concentration of more than 50 ng/mL CCL3/MIP-1α (data not shown). We assume that the difference of the cells and the assay system we adopted may be a cause of this matter. As a result, these secreted molecules could induce chemotaxis of PBMCs. CCL3/MIP-1α is produced by a variety of immune cells such as monocytes and macrophage, and orchestrates acute and chronic inflammatory responses by recruiting proinflammatory cells [15]. CCL3/MIP-1α is considered one of the most important molecules in RA pathology [11,16].

Chemokines expressed in joints can recruit leukocytes and stimulate both fibroblast-like synoviocytes (FLS) and chondrocytes to release inflammatory mediators, including cytokines and MMPs, leading to cartilage degradation and pannus formation. Furthermore, chemokines enhance cell proliferation and angiogenesis, leading to synovial hyperplasia. Chemokines released by leukocytes and FLS, or by the chondrocytes themselves, can induce autocrine/paracrine stimulation of these cells, leading to joint destruction [11].

IL-6 is a pleiotropic cytokine with multiple biological effects on immune regulation, haematopoiesis, inflammation, and oncogenesis [17]. These finding suggest that AIF-1 could be involved with various immune-inflammatory reactions by inducing IL-6 and chemokines in $CD14^+$ PBMCs.

In conclusion, we found that AIF-1 upregulated several CC chemokine genes, leading primarily to release of CCL3/MIP-1α that could induce PBMC migration towards inflamed tissue. Although further work is needed to clarify the molecular mechanism of action of AIF-1, we suggest that AIF-1 may represent a molecular target for the therapy of immune-inflammatory disorders.

Acknowledgment

This study was supported by a Grant-in-Aid for Research (C) (No. 22591080) from The Ministry of Education, Culture, Sports, Science and Technology (MEXT) of Japan.

References

[1] U. Utans, R.J. Arceci, Y. Yamashita, M.E. Russel, Cloning and characterization of allograft inflammatory factor-1: a novel macrophage factor identified in rat cardiac allografts with chronic rejection, J. Clin. Invest. 95 (1995) 2954–2962.
[2] François J.M. Iris, Lydie Bougueleret, Sylvie Prieur, Dominique Caterina, Gwenaël Primas, Virginie Perrot, Jerzy Jurka, Patricia Rodriguez-Tome, Jean Michel Claverie, Jean Dausset, Daniel Cohen, Dense Alu clustering and a potential new member of the NF_B family within a 90 kilobase HLA class III segment, Nat. Genet. 3 (1993) 137–145.
[3] Michael V. Autieri, cDNA cloning of human allograft inflammatory factor-1: tissues distribution, cytokine induction, and mRNA expression in injured rat carotid arteries, Biochem. Biophys. Res. Commun. 228 (1996) 29–376.
[4] Michael V. Autieri, Christopher M. Carbone, Over expression of allograft inflammatory factor-1 promotes proliferation of vascular smooth muscle cells by cell cycle deregulation, Arterioscler. Thromb. Vasc. Biol. 21 (2001) 1421–1426.
[5] Christina Orsmark, Tiina Skoog, Leila Jeskanen, Juha Kere, Ulpu Saarialho-Kere, Expression of allograft inflammatory factor-1 in inflammatory skin disorders, Acta Derm. Venereol. 87 (2007) 223–227.
[6] Francesco Del Galdo, Gerd G. Maul, Sergio A. Jiménez, Carol M. Artlett, Expression of allograft inflammatory factor 1 in tissues from patients with systemic sclerosis and in vitro differential expression of its isoforms in response to transforming growth factor beta, Arthritis Rheum. 54 (2006) 2616–2625.
[7] Aihiro Yamamoto, Eishi Ashihara, Yoko Nakagawa, Hiroshi Obayashi, Mitsuhiro Ohta, Hirokazu Hara, Tetsuo Adachie, Takahiro Seno, Masatoshi Kadoya, Masahide Hamaguchi, Hidetaka Ishino, Masataka Kohno, Taira Maekawa, Yutaka Kawahito, Allograft inflammatory factor-1 is overexpressed and induces fibroblast chemotaxis in the skin of sclerodermatous GVHD in a murine model, Immunol. Lett. 135 (1–2) (2011) 144–150.
[8] Mizuho Kimura, Yutaka Kawahito, Hiroshi Obayashi, Mitsuhiro Ohta, Hirokazu Hara, Tetsuo Adachi, Daisaku Tokunaga, Tatsuya Hojo, Masahide Hamaguchi, Atsushi Omoto, Hidetaka Ishino, Makoto Wada, Masataka Kohno, Yasunori Tsubouchi, Toshikazu Yoshikawa, A critical role for allograft inflammatory factor-1 in the pathogenesis of rheumatoid arthritis, J. Immunol. 178 (2007) 3316–3322.
[9] Hermann J. Schluesener, Karin Seid, Jana Kretzschmar, Richard Meyermann, Allograft inflammatory factor-1 in rat experimental autoimmune encephalomyelitis, neuritis, and uveitis: expression by activated macrophages and microglial cells, Glia 24 (1998) 244–251.
[10] Ying Tian, Surbhi Jain, Sheri E. Kelemen, Michael V. Autieri, AIF-1 expression regulates endothelial cell activation, signal transduction, and vasculogenesis, Am. J. Physiol. Cell Physiol. 296 (2) (2009) C256–C266.
[11] Takuji Iwamoto, Hiroshi Okamoto1, Yoshiaki Toyama, Shigeki Momohara, Molecular aspects of rheumatoid arthritis: chemokines in the joints of patients, FEBS J. 275 (2008) 4448–4455.
[12] Sheri E. Kelemen, Michael V. Autieri, Expression of allograft inflammatory factor-1 in T lymphocytes: a role in T-lymphocyte activation and proliferative arteriopathies, Am. J. Pathol. 167 (2) (2005) 619–626.
[13] Keiko Watano, Kazuya Iwabuchi, Satoshi Fujii, Naoki Ishimori[1], Shinya Mitsuhashi, Manabu Ato, Allograft inflammatory factor-1 augments production of interleukin-6, -10 and -12 by a mouse macrophage line, Immunology 104 (3) (2001) 307–316.
[14] M. Gouwy, S. Struyf, N. Berghmans, C. Vanormelingen, D. Schols, J.V. Damme, CXCR4 and CCR5 ligands cooperate in monocyte and lymphocyte migration and in inhibition of dual-tropic (R5/X4) HIV-1 infection, Eur. J. Immunol. 41 (2011) 963–973.
[15] D.N. Cook, The role of MIP-1 alpha in inflammation and hematopoiesis, J. Leukoc. Biol. 59 (1996) 61–66.
[16] Yoshimi Hatano, Tsuyoshi Kasama, Hideaki Iwabuchi, Ryosuke Hanaoka, Hiroko T. Takeuchi, Lu Jing, Yoshiaki Mori, Kazuo Kobayashi, Masao Negishi, Hirotsugu Ide, Mitsuru Adachi, Macrophage inflammatory protein 1 alpha expression by synovial fluid neutrophils in rheumatoid arthritis, Ann. Rheum. Dis. 58 (5) (1999) 297–302.
[17] T. Kishimoto, The biology of interleukin-6, Blood 74 (1989) 1–10.

Biochemical and Biophysical Research Communications 456 (2015) 785–791

Contents lists available at ScienceDirect

Biochemical and Biophysical Research Communications

journal homepage: www.elsevier.com/locate/ybbrc

Inhibition of osteoclastogenesis by osteoblast-like cells genetically engineered to produce interleukin-10

Kazuki Fujioka [a,b], Tsunao Kishida [a], Akika Ejima [a], Kenta Yamamoto [a,c], Wataru Fujii [b], Ken Murakami [b], Takahiro Seno [b,d], Aihiro Yamamoto [b], Masataka Kohno [b], Ryo Oda [e], Toshiro Yamamoto [c], Hiroyoshi Fujiwara [e], Yutaka Kawahito [b], Osam Mazda [a,*]

[a] Department of Immunology, Kyoto Prefectural University of Medicine, Kyoto, Japan
[b] Inflammation and Immunology, Kyoto Prefectural University of Medicine, Kyoto, Japan
[c] Department of Dental Medicine, Kyoto Prefectural University of Medicine, Kyoto, Japan
[d] Department of Rheumatic Diseases and Joint Function, Kyoto Prefectural University of Medicine, Kyoto, Japan
[e] Department of Orthopaedics, Kyoto Prefectural University of Medicine, Kyoto, Japan

ARTICLE INFO

Article history:
Received 2 December 2014
Available online 13 December 2014

Keywords:
Interleukin-10
Osteoblast
Inflammation
Rheumatoid arthritis
Gene therapy

ABSTRACT

Bone destruction at inflamed joints is an important complication associated with rheumatoid arthritis (RA). Interleukin-10 (IL-10) may suppress not only inflammation but also induction of osteoclasts that play key roles in the bone destruction. If IL-10-producing osteoblast-like cells are induced from patient somatic cells and transplanted back into the destructive bone lesion, such therapy may promote bone remodeling by the cooperative effects of IL-10 and osteoblasts. We transduced mouse fibroblasts with genes for IL-10 and Runx2 that is a crucial transcription factor for osteoblast differentiation. The IL-10-producing induced osteoblast-like cells (IL-10-iOBs) strongly expressed osteoblast-specific genes and massively produced bone matrix that were mineralized by calcium phosphate in vitro and in vivo. Culture supernatant of IL-10-iOBs significantly suppressed induction of osteoclast from RANKL-stimulated Raw264.7 cells as well as LPS-induced production of inflammatory cytokine by macrophages. The IL-10-iOBs may be applicable to novel cell-based therapy against bone destruction associated with RA.

1. Introduction

Rheumatoid arthritis (RA) is a chronic disorder characterized by systemic inflammation and multiple arthritis. In addition to synovial lesions, the bones at the inflamed joints are destructed by activated osteoclasts, resulting in severe pain, deformity and disability in patients. Although the pathogenesis of RA remains to be fully understood, crucial roles are played by proinflammatory cytokines such as IL-1β, IL-6, and TNF-α that are secreted from activated T cells and macrophages [1]. These cytokines also provoke synovial fibroblasts to produce RANKL, which subsequently induces osteoclasts to cause destruction of cartilage and bone [2]. Monoclonal antibodies and soluble receptors that block the pro-inflammatory cytokine signals have been used as biological agents and drastically improved the clinical outcome of RA; however, various adverse events may be associated with the therapies such as serious infection [3]. Meanwhile, any current medication has not succeeded in healing destructive bone, and surgical intervention is required to treat patients with severe joint destruction [4,5]. Therefore, it is necessary to develop a new therapeutic approach to suppress inflammation and archive repair of the destructed bones without causing undesirable adverse events.

IL-10 is a profound immunosuppressive cytokine produced by macrophages, T cells, and certain subsets of B cells and dendritic cells (DCs) [6]. Moreover, IL-10 remarkably prevents generation of osteoclasts through the inhibition of NFATc1 expression [7]. Therefore, IL-10 is regarded as a promising cytokine applicable to anti-rheumatic therapy, due to its powerful activities to suppress inflammation as well as osteoclastogenesis.

A number of reports indicated that systemic administration of IL-10 may provide significant therapeutic benefit to animal models of experimental arthritis [8–10]. Moreover, IL-10 suppresses production of inflammatory cytokines such as IL-1β and TNF-α by

Abbreviations: RA, rheumatoid arthritis; iOBs, induced osteoblast-like cells; IL-10-iOBs, IL-10-producing induced osteoblast-like cells; OCN, osteocalcin; OPN, osteopontin; BSP, bone sialoprotein; ALP, alkaline phosphatase.

* Corresponding author at: Department of Immunology, Kyoto Prefectural University of Medicine, Kamikyo, Kyoto 602-8566, Japan. Fax: +81 75 251 5331.
E-mail address: mazda@koto.kpu-m.ac.jp (O. Mazda).

http://dx.doi.org/10.1016/j.bbrc.2014.12.040
0006-291X/

synovial fluid macrophages of RA patients [11]. In previous clinical trials, IL-10 administration was reported safe and well tolerated, but its therapeutic efficacy for RA was unsatisfactory [12,13]. This may be due to insufficiency of distribution of IL-10 at the joint lesions after systemic administration of the cytokine. Systemic administration of a higher dose of IL-10 could potentially cause cancer development, chronic infection, and Th2-dependent autoimmune disorders that represent lupus-like symptoms [14]. Therefore, local delivery of IL-10 to the inflammatory legions is desirable. Some studies have shown that the cells genetically modified to produce IL-10 were effective in treating experimental arthritis in animals [15,16].

Osteoblasts are crucially involved in bone formation and remodeling through production of calcified bone matrix. We hypothesized that if osteoblast-like cells are engineered to produce IL-10 and transplanted into the destructed bone tissue, such a procedure may offer a great deal of therapeutic benefits to RA patients due to remodeling of bone tissue as well as suppression of articular inflammation. Osteoblast-like cells can be induced from mouse fibroblasts by transducing the Runx2 gene that plays an essential role in osteoblast differentiation [17], and this sort of technology may enable production of patient-specific, induced osteoblast-like cells (iOBs) that are suitable for transplantation therapy.

However, effect of IL-10 on osteoblast differentiation remains controversial. IL-10 gene knockout mice showed loss of alveolar bone and osteopenia-like phenotypes including bone mass reduction [18–20]. In contrast, van Vlasselaer et al. reported that administration of exogenous IL-10 inhibited the osteoblast differentiation from mouse bone marrow cells through the inhibition of TGF-β1 [21,22].

In this context, we examined whether co-transduction of Runx2 and IL-10 genes successfully induced mouse fibroblasts into IL-10-producing osteoblast-like cells with capability to produce bone matrix. We also tested whether the genetically modified cells inhibited production of pro-inflammatory cytokines by activated macrophages as well as induction of osteoclasts.

2. Materials and methods

2.1. Cells

Mouse embryonic fibroblasts (MEFs) were obtained from Balb/c embryos at the gestational age of day 13.5 by digestion with collagenase (NB4G®; Serva, Heidelberg, Germany). MEFs were cultured in DMEM supplemented with 10% fetal bovine serum (FBS), 100 U/mL penicillin, 100 μg/mL streptomycin, and 10 mM non-essential amino acids (standard medium). Raw264.7, A20, and SaOS2 were purchased from RIKEN cell bank (Tsukuba, Japan). Yac1 was maintained in our laboratory. SCC-7 was kindly gifted by Dr. Oya at the Department of Therapeutic Radiology and Oncology, Kyoto University, Japan.

2.2. Retrovirus vectors

The cDNA fragments encoding mouse Runx2 and IL-10 genes were obtained from pFLCI-mouse Runx2 and pFLCI-mouse IL-10 plasmids (Danaform, Kanagawa, Japan), respectively, and inserted into the pMX-puro with GeneArt Seamless Cloning and Assembly (Life Technologies, Carlsbad, CA). The resultant retrovirus vector plasmids, pMX-mRunx2.puro and pMX-mIL10.puro, were transfected into the Plat-E packaging cell line with X-treme Gene 9 (Roche Diagnostics, Basel, Switzerland). Twenty-four hours later, the culture medium was replaced by fresh one, and after incubation for another 24 h, culture supernatant containing retrovirus vectors was harvested.

2.3. Induction of osteoblasts

MEFs were seeded onto a 24-well plate at a density of 1.5×10^4 per well. On the next day, the retrovirus vector suspension was supplemented with 4 μg/mL polybrene (Nacalai Tesque, Kyoto, Japan) and added to the cells, which were subsequently cultured in the standard medium supplemented with 100 nM dexamethasone (Nacalai Tesque), 50 μg/mL L-ascorbic acid (Nacalai Tesque), and 10 mM β-glycerophosphate (Tokyo Chemical Industry, Tokyo, Japan)(osteogenic medium). The culture was continued for 2 to 4 weeks, while the medium was changed every 2 days.

2.4. Alizarin red S staining and staining by von Kossa's method

For Alizarin red S staining, cells were fixed with 95% ethanol for 10 min at room temperature. After washing with distilled water, cells were stained with Alizarin red S solution (Sigma–Aldrich, St. Louis, MO) for 30–45 min, followed by another washing with distilled water. Stained area was calculated with ImageJ [23]. For von Kossa staining, cells were fixed in 10% neutral buffered formalin for 10 min at room temperature. After 3 times washing with distilled water, 5% silver nitrate solution (ScyTek Laboratories, Logan, UT) was added to the cells, which were subsequently exposed to ultra violet for 30–60 min. Culture dishes were rinsed 3 times with distilled water, and incubated with 5% sodium thiosulfate solution (ScyTek Laboratories) for 2 min.

2.5. Alkaline phosphatase (ALP) staining

ALP activity was determined by ALP staining using a Leukocyte Alkaline Phosphatase Kit (Sigma–Aldrich) following the manufacture's instruction. Briefly, cells were fixed with 60% acetone/40% citrate. After washing with deionized water, cells were stained with a diazonium salt solution containing fast violet blue salt and 4% of naphthol AS-MX phosphate alkaline solution for 1 h under protection from light.

2.6. Immunofluorescence staining

Cells were fixed with 4% paraformaldehyde at 4 °C for 30 min, followed by washing with 0.02% Tween-20/PBS. After blocking, cells were washed and incubated with FITC-conjugated rat anti-mouse IL-10 (final concentration was 1:100) (eBioscience, San Diego, CA) and Cy5.5-conjugated rabbit anti-mouse osteocalcin (OCN) (final concentration was 1:100) (Bioss, Woburn, MA) antibodies. On the next day, cells were washed, and observed under a fluorescence microscope.

2.7. Real time RT-PCR

Cells were homogenized in Isogen 2 (Nippongene, Tokyo, Japan), and total RNA was harvested by the phenol guanidinium acid-based procedure. After reverse transcription using ReverTra Ace qPCR RT Master Mix (TOYOBO, Osaka, Japan), cDNA served as template for real time PCR using Applied Biosystems 7300 Real-Time PCR System. The primers and dye probe for osteocalcin (OCN) (Bglap: Mm03413826_mH), osteopontin (OPN) (SPP1: Mm00436767_m1), bone sialoprotein (BSP) (IBSP: Mm00492555_m1), alkaline phosphatase (Alpl: Mm00492555_m1), IL-1β (Il1b: Mm00434228_m1), telomerase reverse transcriptase (Tert: Mm00436931_m1) and β-actin (Mm00607939-m1) genes were purchased from Applied Biosystems (Carlsbad, CA). The primer sequences for TNF-α and IL-6 genes were as follows: TNF-α forward, 5′-tcttctcattcctgcttgtgg-3′; TNF-α reverse, 5′-ggtctgggccatagaactga-3′; IL-6 forward, 5′-gctaccaaactggatataatcagga-3′, IL-6 reverse, 5′-ccaggtagctatggtactccagaa-3′. Corresponding proves were purchased from Roche Applied

Science (Basel, Switzerland) (Universal Probe Library: TNF-α#49, IL-6#6). Samples were incubated at 95 °C for 10 min for an initial denaturation, followed by forty PCR cycles that consisted of denaturation at 95 °C for 15 s and annealing/extension at 60 °C for 1 min. β-actin gene was regarded as endogenous standard and normalization was calculated using RQ software. All experiments were performed in triplicate.

2.8. ELISA

The concentration of IL-10 was measured using Mouse IL-10 Ready SET Go ELISA kit (eBioscience) according to the manufacturer's instruction.

2.9. Induction of osteoclasts

Raw264.7 cells obtained from the RIKEN cell bank were plated in 12-well plates at a density of 1×10^4 cells/well, and cultured in a standard medium supplemented with or without 100 ng/mL of RANKL (PeproTech, Rocky Hill, NJ). In some wells, culture supernatants that had been harvested from MEFs, induced osteoblast-like cells (iOBs), and IL-10-producing iOBs (IL-10-iOBs) were added. The culture medium was replaced by a fresh one on day 3. Six days after the initiation of the culture, cells were subjected to tartrate-resistant acid phosphatase (TRAP) staining using the TRAP kit (Primary Cell, Sapporo, Japan). Briefly, the cells were fixed with 10% neutral buffered formalin for 5 min, followed by incubation at 37 °C for 1 h in 50 mmol/L tetrate buffer containing substrate. After washing with distilled water, the TRAP-positive multi-nuclear cells were regarded as mature osteoclasts.

2.10. Activation of peritoneal macrophages

6–8 week-old female Balb/c mice were intraperitoneally injected with 2 mL of thioglycolate medium. Three days later, mice were sacrificed and 5 mL of PBS was injected into the peritoneal cavity. After gentle massage, the peritoneal exudate cells were retrieved and seeded into 12-well plates at 1.5×10^6 cells per well. After 2 h of culture, the floating cells were removed, and residual adherent cells were cultured for 24 h in the presence of supernatants of MEFs, iOBs and IL-10-iOBs. Cells were then stimulated with LPS (100 ng/mL)(Invitrogen, Carlsbad, CA) for 2 h.

2.11. Contact inhibition

SaOS2 cells and MEFs that had been transduced with Runx2 and IL-10 genes were seeded in 60 mm culture dishes at a density of 1.5×10^5 cells/dish, and cultured for 15 days without trypsinization and reseeding. Cell morphology was observed under phase-contrast microscopy.

2.12. Transplantation

Twenty-four hours after infection with the Runx2 and/or IL-10 retrovirus vectors, MEFs, iOBs and IL-10-iOBs were seeded on hydrogel scaffold (MedGel® SP; MedGEL, Tokyo, Japan) at a density of 3.5×10^4 cells/scaffold. After pre-culture for 2 days in osteogenic medium, the cells were subcutaneously transplanted into the flank of 6-week-old female Balb/c mice. Four weeks later, the graft was excised and cryosectioned. Mineralization status of the specimens was estimated by Alizarin red staining and staining by the von Kossa's method as above. To examine tumor formation, IL-10-iOBs or MEFs that had been cultured in osteogenic medium for 2 days were subcutaneously inoculated into 7-week-old male SCID/NOD mice with or without hydrogel scaffold at a dose of either 3.5×10^4 or 3.0×10^6/mouse.

2.13. Statistical Analysis

All the data were analyzed by Student's unpaired *t*-test, and $p < 0.05$ was considered statistically significant.

3. Results

3.1. IL-10 gene transduction did not prevent Runx2-mediated induction of osteoblast-like cells from fibroblasts

To generate IL-10-secreting osteoblast-like cells, we transduced primary mouse embryonic fibroblasts (MEFs) with Runx2 and IL-10 genes via retrovirus vectors, and analyzed the phenotypes of the resultant cells (IL-10-iOBs) in comparison with those of the osteoblast-like cells induced by transduction of Runx2 gene alone (iOBs). The ALP staining indicated that both IL-10-iOBs and iOBs showed high activities of ALP, an early stage marker of osteoblast differentiation, 10 days after the gene transduction (Fig. 1A, top). Alizarin red S staining unveiled that the IL-10-iOBs produced mineralized bone matrix as massively as iOBs on day 20, whereas un-transduced MEFs failed to show any significant staining (Fig. 1A, middle). Calculation of the Alizarin red S-stained areas also demonstrated comparable degrees of calcification in IL-10-iOBs and iOBs cultures (data not shown). Staining by the von Kossa's method also confirmed massive calcium deposition by IL-10-iOBs and iOBs, but not by MEFs (Fig. 1A, bottom).

To further confirm the osteoblast-like characteristics of the cells, we examined expression of osteoblast marker genes 15 days after the gene transfer (Fig. 1B). Quantitative RT-PCR analysis demonstrated that IL-10-iOBs expressed similar or even higher levels of mRNA for the osteocalcin (OCN), osteopontin (OPN), bone sialoprotein (BSP) and ALP genes as iOBs.

These data strongly suggested that IL-10 gene transfer did not hamper osteoblast-like phenotypic conversion of MEFs.

3.2. IL-10-iOBs produced IL-10 at a high level

To assess the IL-10 production by IL-10-iOBs, we performed quantitative RT-PCR 15 days after the initiation of the osteoblast induction. The cells expressed a high level of IL-10 mRNA, which was not the case with iOBs and MEFs (Fig. 2A). We also harvested the supernatants of the IL-10-iOBs and measured IL-10 concentrations by ELISA, which showed robust IL-10 secretion from the cells on days 1 and 2 (Fig. 2B).

Because IL-10-iOBs potentially contained heterogeneous populations, further experiments were performed to clarify whether the IL-10 was produced by the cells with osteoblast-like features. Immunofluorescence staining of IL-10-iOBs was performed to visualize OCN and IL-10 on day 14. As shown in Fig. 2C, OCN and IL-10 were co-localized in the same cells, indicating that IL-10 was produced by the osteoblast-like cells.

3.3. Conditioned medium of IL-10-iOBs suppressed induction of osteoclasts

To estimate whether the IL-10 secreted from IL-10-iOBs was capable of inhibiting osteoclastogenesis, we collected the culture supernatants of the IL-10-iOBs, iOBs and MEFs, and examined their effect on the mouse macrophage cell line, Raw264.7, that was induced to differentiate into osteoclasts by an addition of RANKL [24,7]. Six days after the induction, a number of TRAP-stained multinuclear cells (MNCs) appeared in the cultures in which the supernatant of MEFs or iOBs had been added (Fig. 3A). In contrast, the

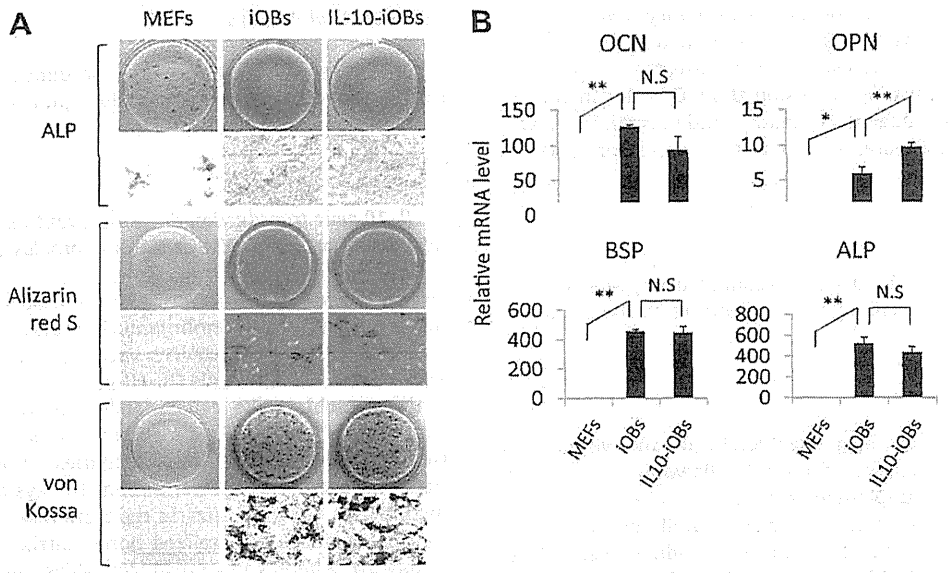

Fig. 1. Transduction of IL-10 gene did not inhibit induction of osteoblast-like phenotypes in MEFs. MEFs were infected with Runx2 (iOBs) and both Runx2 and IL-10 (IL-10-iOBs) retrovirus vectors. (A) Cells were cultured for 10 days and subjected to the ALP staining (top), while the other aliquots of cells were cultured for 20 days and subjected to the Alizarin red S staining (middle) or to staining by von Kossa's method (bottom). Gross appearance (upper) and microscopic images at magnification of ×100 (lower) are shown. (B) Fourteen days after gene transfer, RNA was extracted from the cells, and qRT-PCR analysis was performed to evaluate mRNA levels for osteocalcin (OCN), osteopontin (OPN), bone sialoprotein (BSP) and ALP genes. Data represent the means ± SD ($n = 3$). $^{*}p < 0.05$, $^{**}p < 0.01$, N.S.: not significant.

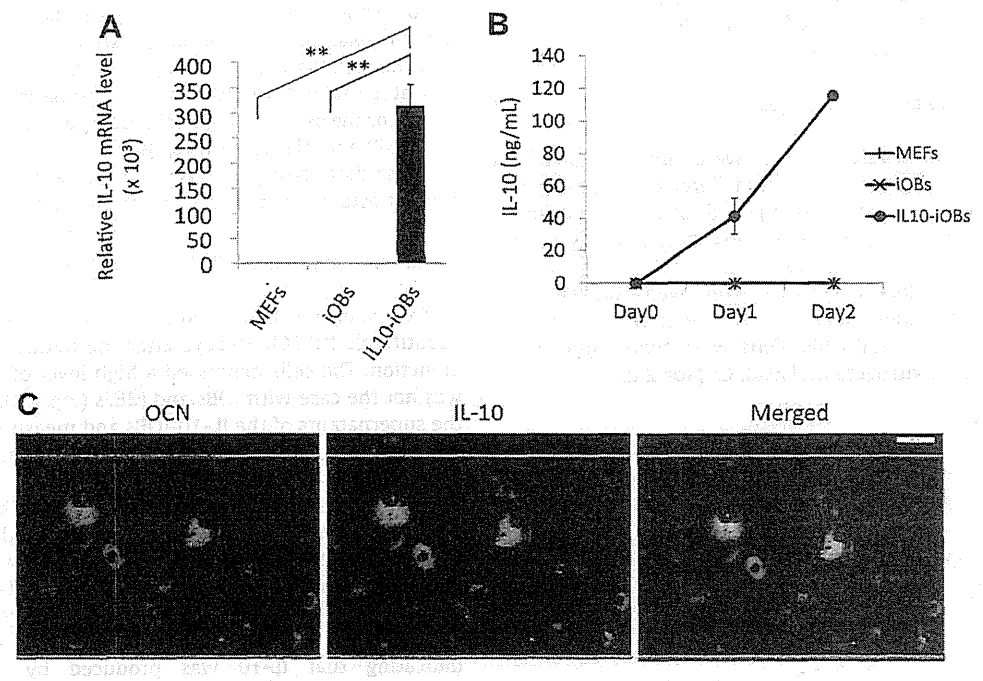

Fig. 2. IL-10-iOBs produced a large amount of IL-10. (A) RNA was extracted from MEFs, iOBs and IL-10-iOBs 14 days after gene transduction, and qRT-PCR analysis was performed to evaluate IL-10 mRNA. Data represent the means ± SD ($n = 3$). $^{**}p < 0.01$. (B) Culture supernatants of MEFs, iOBs, and IL-10-iOBs were harvested at the indicated days, and the concentrations of IL-10 were measured by ELISA. Data represent the means ± SD ($n = 3$). $^{**}p < 0.01$. (C) IL-10-iOBs were immunostained using FITC-conjugated anti-IL-10 and Cy5.5-conjugated anti-OCN antibodies 14 days after gene transfer. Scale bar shows 50 μm.

osteoclast-like cells were hardly detectable in the culture that had received the supernatant of the IL-10-iOBs. We counted the number of TRAP-positive MNCs in each group and confirmed that an addition of supernatant of IL-10-iOBs significantly reduced the number of osteoclast-like cells induced from Raw264.7 cells (Fig. 4B).

3.4. Conditioned medium of IL-10-iOBs suppressed production of inflammatory cytokines by activated macrophages

We examined the effect of IL-10-iOB supernatant on cytokine production by activated macrophages. The thioglycollate-elicited peritoneal macrophages were cultured with supernatant of IL-10-

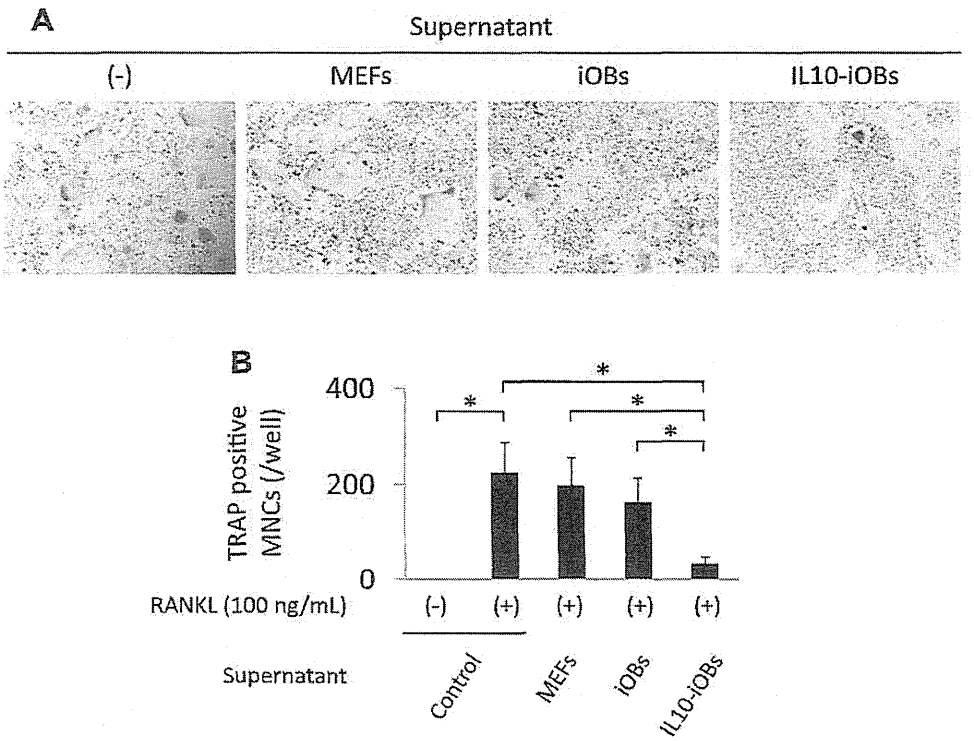

Fig. 3. Culture supernatant of IL-10-iOBs suppressed differentiation of RANKL-stimulated Raw264.7 cells into osteoclasts. Raw264.7 cells were cultured with RANKL and supernatant of the indicated cells. Six days later, cells were subjected to TRAP staining. (A) Microscopic images at magnification of ×100 are shown. (B) The numbers of TRAP-positive multi-nuclear cells (MNCs) per well are plotted. Data represent the means ± SD ($n = 3$). $^{*}p < 0.05$, $^{**}p < 0.01$.

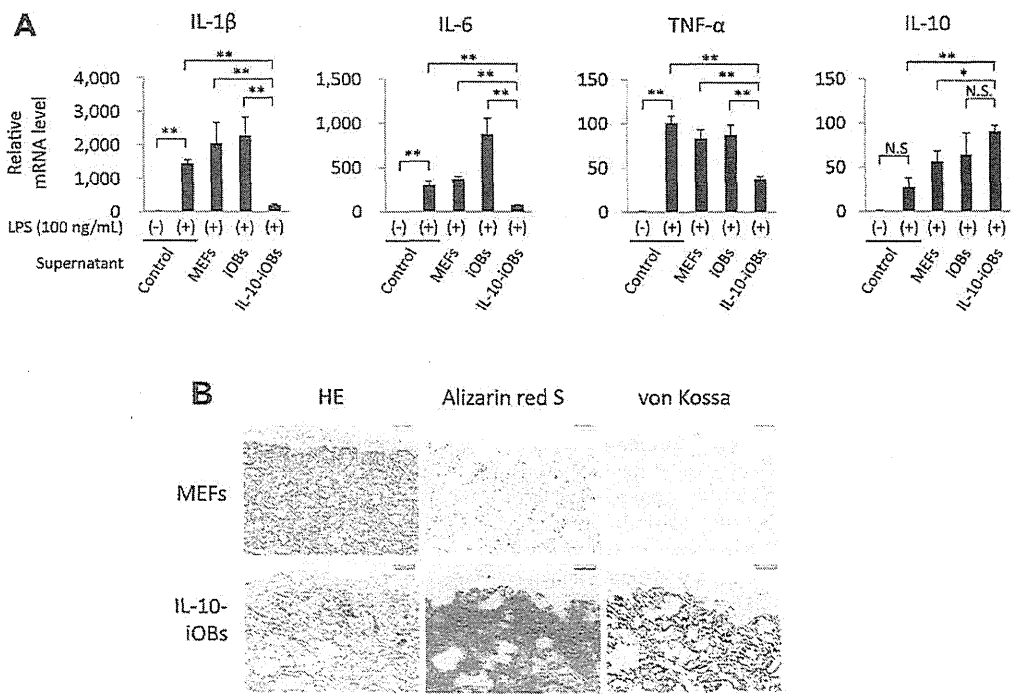

Fig. 4. Culture supernatant of IL-10-iOBs prevented LPS-stimulated macrophages from producing proinflammatory cytokines, while IL-10-iOBs produced mineralized bone matrix in vivo. (A) Peritoneal macrophages were cultured with the supernatants of the indicated cells, and stimulated with LPS as described in the materials and methods. Two hours later, RNA was extracted from the cells and mRNA for the indicated cytokines was evaluated by qRT-PCR. Data represent the means ± SD ($n = 3$). $^{*}p < 0.05$, $^{**}p < 0.01$, N.S., not significant. (B) MEFs were transduced with Runx2 and IL-10 genes and seeded on hydrogel scaffold. After culturing for 2 days, the cells and scaffold were transplanted into the flank mice. Graft was excised 4 weeks later, and tissue was subjected to the indicated staining (Scale bars indicate 100 μm).

iOBs, iOBs or MEFs, followed by stimulation with 100 ng/mL LPS. 2 h later, mRNA levels for IL-1β, IL-6, TNF-α and IL-10 were evaluated by real time RT-PCR. As shown in Fig. 4A, the supernatant of IL-10-iOBs significantly suppressed mRNA expression of IL-1-β, IL-6 and TNF-α. Neither MEF nor iOB supernatants significantly affected the expression of the pro-inflammatory cytokines, except that the supernatant of iOBs significantly enhanced IL-6 mRNA expression. In sharp contrast, the supernatant of IL-10-iOBs rather elevated the expression of IL-10 mRNA by the LPS-stimulated macrophages.

These results strongly suggested that IL-10 secreted from IL-10-iOBs suppressed production of the pro-inflammatory cytokines.

3.5. Significant bone formation in vivo by ectopically transplanted IL-10-iOBs

We tested whether the IL-10-iOBs are capable of forming bone in vivo. The IL-10-iOBs cultured on hydrogel scaffold were subcutaneously transplanted into the flank of the syngenic mice. After 4 weeks, histological assessment of the graft was performed, and the specimen was strongly stained with Alizarin red S (Fig. 4B, lower middle). The bone formation was also confirmed by the positive staining by the von Koss's method (Fig. 4B, lower right), while the HE staining did not show any sign of inflammatory cell infiltration (Fig. 4B, lower left). Meanwhile, bone formation was totally absent in the tissue into which MEFs had been transplanted as a control (Fig. 4B, upper).

Therefore, IL-10-iOBs remarkably produced a mineralized bone matrix in vivo after transplantation, suggesting applicability of the cells to novel cell therapy for RA.

3.6. IL-10-iOBs lacked tumor-like characteristics

Finally, we examined whether IL-10-iOBs exhibited tumor cell-like features. In culture, IL-10-iOBs proliferated until they form a confluent monolayer and subsequently underwent growth arrest (Supplementary Fig. 1A). This is in sharp contrast to SaOS2 osteosarcoma cells that showed loss of contact inhibition. The IL-10-iOBs expressed mRNA for the telomerase reverse transcriptase (TERT) gene at as low level as fibroblasts, whereas most tumor cells highly expressed TERT (Supplementary Fig. 1B) [25].

Tumorigenic potential of IL-10-iOBs was assessed by subcutaneously inoculation into immune-deficient mice. Tumor development was not seen in all the mice. Taken together, it was strongly suggesting that the IL-10-iOBs did not have tumorigenicity (Supplementary Table S1).

4. Discussion

In the present study, we proposed a novel therapeutic procedure for RA based on the transplantation of genetically modified osteoblast-like cells. By transducing MEFs with the genes for osteoblast differentiation factor Runx2 and potent anti-inflammatory cytokine IL-10, the established IL-10-iOBs expressed osteoblast marker genes at high levels (Fig. 1B) and massively produced mineralized bone matrix both in vitro (Fig. 1A) and in vivo (Fig. 4B), while IL-10 was also abundantly produced by the osteocalcin-positive cells (Fig. 2), strongly suggesting that IL-10 production did not interfere with Runx2-mediated induction of the osteoblast-like phenotypes. Previous reports indicated that administration of IL-10 suppressed differentiation of osteoblasts through inhibition of the TGF-β signaling [22], while TGF-β signaling contributes to osteoblast differentiation by inducing Runx2 expression [26]. Therefore, exogenous Runx2 gene may have substituted for the endogenous Runx2 that was suppressed by IL-10, resulting in restoration of the IL-10-mediated interference of osteoblast differentiation.

The supernatant of IL-10-iOBs significantly suppressed both RANKL-mediated induction of osteoclasts from Raw264.7 (Fig. 3) and production of inflammatory cytokines by LPS-activated macrophages (Fig. 4A). The anti-inflammatory and anti-osteoclast functions of the IL-10-iOBs may cooperatively ameliorate the inflammatory bone destruction at the joint lesions of RA patients, if transplantation therapy using these cells is clinically applicable to RA patients in the future. An extremely high production of IL-10 may cause some adverse events such as immunosuppression. To limit the serum level of IL-10 not to exceed the tolerable level, patients may be transplanted with a mixture of IL-10-iOBs and iOBs at an appropriate ratio.

The iOBs may be quite adequate for the cell-based therapy for RA, because a sufficient number of iOBs with high bone formation capacity may be induced from patients' own somatic cells. Fibroblasts may be particularly useful as the somatic cells to be induced into iOBs, because they can be obtained from RA patients in a minimally invasive fashion and allowed to proliferate to a large number in culture before induction into osteoblast-like cells. Other cells such as leukocytes may become an alternative for fibroblasts, but this point should be examined in further studies. Although the transduction of Runx2 gene alone fails to induce osteoblast-like phenotypic change in somatic cells of human origin, this problem may be overcome by using some combinations of genes instead of Runx2 gene alone, and we have already established such a procedure (Yamamoto et al., a manuscript submitted for publication).

Acknowledgments

This work was supported by grants from the Japan Science and Technology Agency, and the Japanese Ministry of Education, Culture, Sports, Science and Technology. All authors have declared there are no financial conflicts of interest in regards to this study.

Appendix A. Supplementary data

Supplementary data associated with this article can be found, in the online version, at http://dx.doi.org/10.1016/j.bbrc.2014.12.040.

References

[1] I.B. McInnes, G. Schett, Cytokines in the pathogenesis of rheumatoid arthritis, Nat. Rev. Immunol. 7 (2007) 429–442.
[2] Y. Wu, J. Liu, X. Feng, et al., Synovial fibroblasts promote osteoclast formation by RANKL in a novel model of spontaneous erosive arthritis, Arthritis Rheum. 52 (2005) 3257–3268.
[3] V. Connor, Anti-TNF therapies: a comprehensive analysis of adverse effects associated with immunosuppression, Rheumatol. Int. 31 (2011) 327–337.
[4] U. Møller Døhn, A. Boonen, M.L. Hetland, et al., Erosive progression is minimal, but erosion healing rare, in patients with rheumatoid arthritis treated with adalimumab. A 1 year investigator-initiated follow-up study using high-resolution computed tomography as the primary outcome measure, Ann. Rheum. Dis. 68 (2009) 1585–1590.
[5] S. Finzel, J. Rech, S. Schmidt, et al., Interleukin-6 receptor blockade induces limited repair of bone erosions in rheumatoid arthritis: a micro CT study, Ann. Rheum. Dis. 72 (2013) 396–400.
[6] M. Saraiva, A. O'Garra, The regulation of IL-10 production by immune cells, Nat. Rev. Immunol. 10 (2010) 170–181.
[7] K.E. Evans, S.W. Fox, Interleukin-10 inhibits osteoclastogenesis by reducing NFATc1 expression and preventing its translocation to the nucleus, BMC Cell Biol. 8 (2007) 4.
[8] L. Ye, Z. Wen, Y. Li, et al., Interleukin-10 attenuation of collagen induced arthritis is associated with suppression of interleukin-17 and retinoid related orphan receptor γt production in macrophages and repression of classically activated macrophages, Arthritis Res. Ther. 16 (2014) R96.
[9] N.A. Carter, E.C. Rosser, C. Mauri, Interleukin-10 produced by B cells is crucial for the suppression of Th17/Th1 responses, induction of T regulatory type 1 cells and reduction of collagen-induced arthritis, Arthritis Res. Ther. 14 (2012) R32.

[10] M. Walmsley, P.D. Katsikis, E. Abney, et al., Interleukin-10 inhibition of the progression of established collagen-induced arthritis, Arthritis Rheum. 39 (1996) 495–503.
[11] P.H. Hart, M.J. Ahern, M.D. Smith, et al., Comparison of the suppressive effects of interleukin-10 and interleukin-4 on synovial fluid macrophages and blood monocytes from patients with inflammatory arthritis, Immunology 84 (1995) 536–542.
[12] K. Asadullah, W. Sterry, H.D. Volk, Interleukin-10 therapy–review of a new approach, Pharmacol. Rev. 55 (2003) 241–269.
[13] K.W. Moore, R. de Waal, Malefyt R.L. Coffman, Interleukin-10 and the interleukin-10 receptor, Annu. Rev. Immunol. 19 (2001) 683–765.
[14] E. Bijjiga, A.T. Martino, Interleukin 10 (IL-10) regulatory cytokine and its clinical consequences, J. Clin. Cell Immunol. S1 (2013) 007.
[15] K. Setoguchi, Y. Misaki, Y. Araki, et al., Antigen-specific T cells transduced with IL-10 ameliorate experimentally induced arthritis without impairing the systemic immune response to the antigen, J. Immunol. 165 (2000) 5980–5986.
[16] L. Henningsson, T. Eneljung, P. Jirholt, et al., Disease-dependent local IL-10 production ameliorates collagen induced arthritis in mice, PLoS ONE 7 (2012) e49731.
[17] J.E. Phillips, R.E. Guldberg, A.J. García, Dermal fibroblasts genetically modified to express Runx2/Cbfa1 as a mineralizing cell source for bone tissue engineering, Tissue Eng. 13 (2007) 2029–2040.
[18] M. Claudino, T.P. Garlet, C.R. Cardoso, Down-regulation of expression of osteoblast and osteocyte markers in periodontal tissues associated with the spontaneous alveolar bone loss of interleukin-10 knockout mice, Eur. J. Oral Sci. 118 (2010) 19–28.
[19] A. Al-Rasheed, H. Scheerens, D.M. Rennick, et al., Accelerated alveolar bone loss in mice lacking interleukin-10, J. Dent. Res. 82 (2003) 632–635.
[20] R. Dresner-Pollak, N. Gelb, D. Rachmilewitz, et al., Interleukin 10-deficient mice develop osteopenia, decreased bone formation, and mechanical fragility of long bones, Gastroenterology 127 (2004) 792–801.
[21] P. Van Vlasselaer, B. Borremans, R. Van Den Heuvel, et al., Interleukin-10 inhibits the osteogenic activity of mouse bone marrow, Blood 82 (1993) 2361–2370.
[22] P. Van Vlasselaer, B. Borremans, U. van Gorp, et al., Interleukin 10 inhibits transforming growth factor-beta (TGF-beta) synthesis required for osteogenic commitment of mouse bone marrow cells, J. Cell Biol. 124 (1994) 569–577.
[23] C.A. Schneider, W.S. Rasband, K.W. Eliceiri, NIH Image to ImageJ: 25 years of image analysis, Nat. Methods 9 (2012) 671–675.
[24] S.G. Mohamed, E. Sugiyama, K. Shinoda, et al., Interleukin-10 inhibits RANKL-mediated expression of NFATc1 in part via suppression of c-Fos and c-Jun in RAW264.7 cells and mouse bone marrow cells, Bone 41 (2007) 592–602.
[25] E.H. Blackburn, Telomerase and cancer, Mol. Cancer Res. 3 (2005) 477–482.
[26] K.S. Lee, H.J. Kim, Q.L. Li, et al., Runx2 is a common target of transforming growth factor beta1 and bone morphogenetic protein 2, and cooperation between Runx2 and Smad5 induces osteoblast-specific gene expression in the pluripotent mesenchymal precursor cell line C2C12, Mol. Cell. Biol. 20 (2000) 8783–8792.

Clin Rheumatol (2014) 33:911–917
DOI 10.1007/s10067-014-2526-1

ORIGINAL ARTICLE

Maximum intensity projection with magnetic resonance imaging for evaluating synovitis of the hand in rheumatoid arthritis: comparison with clinical and ultrasound findings

Daigo Taniguchi · Daisaku Tokunaga · Ryo Oda · Hiroyoshi Fujiwara · Takumi Ikeda · Kazuya Ikoma · Aiko Kishida · Tetsuro Yamasaki · Yutaka Kawahito · Takahiro Seno · Hirotoshi Ito · Toshikazu Kubo

Received: 21 August 2013 / Revised: 27 December 2013 / Accepted: 3 February 2014 / Published online: 6 March 2014

Abstract Magnetic resonance imaging (MRI) with maximum intensity projection (MIP) is used to evaluate the hand in rheumatoid arthritis (RA). MIP yields clear visualization of synovitis over the entirety of the bilateral hands with a single image. In this study, we assessed synovitis with MIP images, clinical findings, and power Doppler (PD) findings to examine the clinical usefulness of MIP images for RA in the hand. Thirty RA patients were assessed for swelling and tenderness in the joints included in the DAS28, and both contrast-enhanced MRI for bilateral hands and ultrasonography for bilateral wrist and metacarpophalangeal (MCP) joints were performed. Articular synovitis was scored in MIP images, and the scores were compared with those for PD. The agreement on synovitis between MIP and conventional MR images was excellent. Palpation showed low sensitivity and high specificity compared with both MIP and PD images. There were joints that were positive in MIP images only, but there were no joints that were positive in PD images only. A statistically significant correlation between the scores of MIP and PD images was found. Furthermore, the agreement between grade 2 on MIP images and positive on PD images was 0.87 (κ=0.73) for the wrist and 0.92 (κ=0.57) for MCP joints. Using MIP images together with palpation makes detailed evaluation of synovitis of the hand in RA easy. MIP images may predict further joint damage, since they allow semiquantitative estimation of the degree of thickening of the synovial membrane.

Keywords Hand · Magnetic resonance imaging · Maximum intensity projection · Rheumatoid arthritis · Synovitis · Ultrasonography

D. Taniguchi · D. Tokunaga · R. Oda (✉) · H. Fujiwara · T. Ikeda · K. Ikoma · A. Kishida · T. Yamasaki · T. Kubo
Department of Orthopaedics, Graduate School of Medical Science, Kyoto Prefectural University of Medicine, Kawaramachi-Hirokoji, Kamigyo-ku, Kyoto 602-8566, Japan
e-mail: roda@koto.kpu-m.ac.jp

Y. Kawahito · T. Seno
Department of Inflammation and Immunology, Graduate School of Medical Science, Kyoto Prefectural University of Medicine, Kyoto, Japan

T. Seno · T. Kubo
Department of Rheumatic Diseases and Joint Function, Kyoto Prefectural University of Medicine, Kyoto, Japan

H. Ito
Department of Diagnostic Radiology, Kajiicho Medical Imaging Center, Kyoto, Japan

Introduction

The hand is the most common site of rheumatoid arthritis (RA), therefore evaluation of arthritis at this site is important for diagnosis and estimation of disease activity. Physical findings and conventional radiographs have been used to evaluate the hands in RA; however, more precise methods of evaluation are now needed because of remarkable advances in RA treatment in recent years [1, 2]. As new imaging methods, magnetic resonance imaging (MRI) and joint ultrasonography (US) are currently used in RA [3]. Synovial inflammation and bone edema can be confirmed with contrast-enhanced MRI, which is not possible with plain radiographs, and it can confirm bone erosion at an earlier stage than plain radiographs [3, 4]. The correlation between synovial membrane thickness and joint destruction has been reported, and several methods to quantify thickness with contrast-enhanced MR images have been reported [5–8]. However, these methods take too long to use during outpatient treatment because quantification involves interpretation of numerous images.

We have used contrast-enhanced MR images and the images processed with maximum intensity projection (MIP), together with physical findings and plain radiographs, to evaluate the hands in RA since 2002 [9]. MIP is a method of image processing in which the brightest regions of different slices are superimposed on each other to create a single three-dimensional (3D) image [10–12]. MIP images of the hand in RA provide clear visualization of synovitis and also enable differentiation of articular synovitis and tenosynovitis anatomically [13–15]. A single MIP image of the hands allows observation of the whole of both hands, like plain radiographs. For these reasons, synovitis can be diagnosed easily in MIP images; additionally, the distribution of synovitis is very important for diagnosing whether the synovitis is due to RA, infection or other arthritis, because RA is a disease with polyarthritis [9, 13]. The time required for interpretation is less than 1/4 of that with regular contrast-enhanced MR images, and the diagnostic accuracy is equivalent to that with regular images [14]. Clinically, to diagnose precisely and efficiently, we first assess MIP images and then we check conventional MR images with reference to the MIP images. Incorporating MIP images in picture archive and communication systems (PACS) or other image systems permits easy review of the synovitis and makes it easier for both physicians and patients to understand the state of disease.

As well as MR images, we have recently been using US to evaluate synovitis. In general, gray scale (GS) and power Doppler (PD) images are recorded with US. PD-positive synovitis, in particular, is important because the findings are considered to indicate progressive joint destruction, even if the patient is in clinical remission [8, 16–19]. In this study, we compared MIP images, palpation findings, and PD findings of synovitis to examine the clinical usefulness of MIP images for evaluating the hands in RA. We also used a simple method to score MIP images of synovitis in the hands in RA and compared these scores with those from PD images to examine the clinical significance of synovitis on MIP images.

Materials and methods

Patients

Thirty RA patients were included in the study. All patients fulfilled the American Rheumatism Association 1987 criteria for RA [20]. For future prospective studies, we selected patients who were not receiving biological agents or oral doses of steroids. Tenderness and swelling in the 28 joints in the disease activity score (DAS)28 [21] were recorded, and C-reactive protein (CRP) levels were obtained; the DAS28-CRP was then calculated from these data to evaluate disease activity in each patient. All patients were examined using both MRI and US.

All patients gave informed consent, and the study was approved by the local Research Ethics Committee of our hospital.

MIP images

All MRI examinations of hands were performed in the supine position using a 1.5-T clinical scanner (EXCELART Vantage powered by Atlas; Toshiba, Japan), with the Atlas SPEEDER 16-channel phased array coil. Patients placed both hands on the front of their thighs. Before obtaining the contrast-enhanced fat-suppressed 3D T1-weighted images (T1WI), we obtained non-contrast-enhanced STIR, T1WI, and T2WI with coronal orientation. In all patients, an intravenous bolus of 0.1 mmol gadoteridol/kg body weight (Prohance, Eisai, Japan, Tokyo) was injected, and then, fat-suppressed contrast-enhanced 3D gradient echo T1WI were started acquisition within 3 min of injection of the contrast medium. A fat-suppressed 3D gradient echo T1WI sequence was conducted with the following parameters: repetition time/echo time (TR/TE)=5.5/2.5 ms, number of acquisitions=1, slice thickness=2 mm, field-of-view=350×350 mm, acquisition matrix=256×256, and acquisition time=approximately 3 min 40 s. The MIP images were post-processed from fat-suppressed 3D gradient echo T1WI. In MIP images, each joint (wrist, metacarpophalangeal [MCP] joint and proximal interphalangeal [PIP] joint) was scored separately for the presence of articular synovitis on a semiquantitative scale. Since there are no previous reports of a scoring method, we used an original scale from 0 to 2 (grade 0=no enhancement, grade 1=partial enhancement of the joint, grade 2=complete enhancement of the joint) (Fig. 1). We considered grade 1 or 2 to be positive for articular synovitis. Furthermore, we scored articular synovitis with fat-suppressed contrast-enhanced 3D gradient echo T1WI with reference to a previous report [14], in order to compare with the MIP scores. Two orthopedic surgeons specializing in RA conducted scoring independently, without reference to any other clinical information.

Power doppler images

US was performed on the wrist and MCP joints using a HI VISION Avius (Hitachi Medical Corporation, Tokyo, Japan) with a linear type (14–6 MHz) probe. Patients were examined while seated with the hand placed on a cushion and pronated. The dorsal side of the hand was scanned in the longitudinal plane. Radial images of the wrist were taken with Lister's tubercle and the second metacarpal bone as landmarks, medial images of the wrist were taken around the center of the wrist, and ulnar images of the wrist were taken with the head of the ulna as the landmark. Images of the MCP joint were taken around the center of each joint. We searched for the most active area of inflammation near these landmarks. GS images

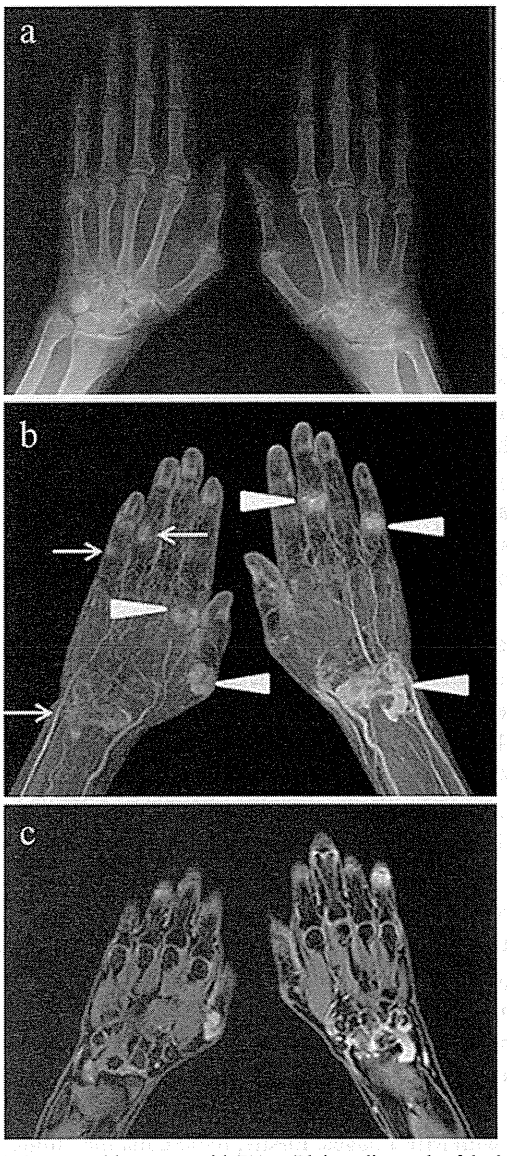

Fig. 1 A 67-year-old woman with RA. **a** Plain radiograph of the hands. **b** MIP image of the hands. Synovitis grade 1 (*arrows*) and grade 2 (*arrowheads*). **c** Contrast-enhanced fat-suppressed T1-weighted image of the hands

with low echo regions within joints were considered to indicate thickening of the synovial membrane. In PD images, the presence of vascular signals was examined. When performing PD evaluation, the receiver gain settings were controlled to eliminate the appearance of artifacts on each joint. The PD frequency was set at 7.5 MHz, and the pulse repetition frequency was set between 800 Hz and 1,000 Hz, optimized for US of rheumatoid hands by the manufacturer. For PD images, each joint was scored on a semiquantitative scale with a score of grade 1 or higher taken as positive (grade 0=no flow in the synovium, grade 1=single vessel signals, grade 2=confluent vessel signals in less than half of the area of the synovium, grade 3=vessel signals in more than half of the area of the synovium) [22]. Intensive training is required for adequate assessment of rheumatoid hands [23, 24]. Therefore, all US examinations were performed by the same orthopedic surgeon who was trained in the examination of the small joints of rheumatoid hands. Two other orthopedic surgeons specializing in RA scored the joints independently, with no reference to any other clinical information.

Statistical analysis

The baseline characteristics of our study group are described as mean values for continuous variables including standard deviations. The agreement was estimated using the weighted kappa statistic. A κ value of 0–0.40 denotes poor agreement, 0.41–0.60 moderate, 0.61–0.80 substantial, and 0.81 or higher excellent agreement [20]. The correlation between two imaging scores was estimated using Spearman's rank correlation coefficient test. To estimate the agreement between two imaging methods, final score decision was made after discussion between the two examiners. Statistical analysis was performed using the Ekuseru-Toukei 2012 software for Windows (Social Survey Research Information Co., Ltd.,Tokyo, Japan).

Results

Our study included 25 women and 5 men. Their mean age was 61.5±9.5 years (range 38–81 years), and their mean disease duration was 12.5±11.5 years (range 4 months–45 years). Twenty-seven patients were being treated with methotrexate, at a mean dose of 7.3±3.1 mg (range 2–14 mg). Steinbrocker classifications were stage 1 for 6 patients, stage 2 for 11, stage 3 for 7, and stage 4 for 6, and class 1 for 13, class 2 for 13, class 3 for 3, and class 4 for 1. The mean DAS28-CRP score for the study group was 2.23±1.01 (range 0.96–5.37). There were 18 patients in remission with DAS28-CRP scores of lower than 2.3, 1 with low disease activity with a score of 2.3–2.7, 10 with moderate disease activity with scores of 2.7–4.1, and 1 with high disease activity with a score of more than 4.1.

A total of 60 wrists and 300 MCP joints were evaluated with clinical examination, MRI, and US. Three hundred PIP joints (including 60 interphalangeal [IP] joints in the thumb) were evaluated with clinical examination and MRI. Interobserver agreement was excellent for MIP image scores, conventional MRI scores, and PD image scores with a κ value of more than 0.81 at each joint area. There were statistically significant correlations between the scores for MIP images and conventional MR images for the wrist (r_s=0.904, P<0.001), MCP joints (r_s=0.919, P<0.001), and PIP joints (r_s=0.930, P<0.001). Furthermore, the κ value for synovitis scores from MIP images and conventional MR images was 0.92 for the wrist, 0.88 for MCP joints, and 0.88 for PIP joints.

Therefore, the agreement on synovitis scores between MIP images and conventional MR images was excellent.

Synovitis was visualized on MIP images in 48 (wrist), 84 (MCP), and 59 (PIP) joints, whereas only 25 (wrist), 26 (MCP), and 10 (PIP) joints exhibited synovitis on clinical assessment (swelling or tenderness) (Fig. 2). Using either MIP or PD images as the reference, clinical examination showed low sensitivity and high specificity in each joint area (Table 1). Using MIP images as a reference, the sensitivity of palpation was 0.52 for the wrist, 0.26 for MCP joints, and 0.12 for PIP joints; thus, the smaller the joint, the lower the sensitivity of palpation (Table 1).

The number of joints positive on MIP images and PD images is shown in Table 2. In PD images, 31 wrists and 23 MCP joints were positive for synovitis, all of which were also positive in MIP images; there were joints that were positive in MIP images only, but there were no joints that were positive in PD images only (Table 2). There were statistically significant correlations between the scores for MIP images and PD images for both wrists (r_s=0.701, P<0.001) and MCP joints (r_s= 0.518, P<0.001). The agreement on synovitis between MIP and PD images was moderate at 0.73 (κ=0.44) for the wrist and poor at 0.80 (κ=0.35) for MCP joints. However, the agreement between grade 2 on MIP images and positive on PD images was substantial at 0.87 (κ=0.73) for the wrist and moderate at 0.92 (κ=0.57) for MCP joints.

Discussion

Clinical findings are essential for evaluating disease activity, but our results show that MIP imaging is more sensitive than palpation in detecting synovitis. This finding is consistent with previous studies regarding imaging of the joints in RA [3, 9, 15, 21, 25–28]. It is also known that most RA patients who satisfied the remission criteria with normal findings on clinical and laboratory studies had imaging-detected synovitis

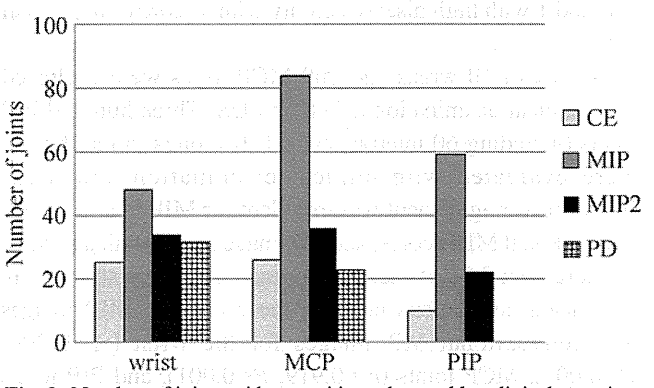

Fig. 2 Number of joints with synovitis as detected by clinical examination, MIP images, and PD images. N=60 (wrist), 300 (MCP), 300 (PIP). *CE*, clinical examination; *MIP*, MIP grades 1 or 2; *MIP2*, MIP grade 2; *PD*, power Doppler

Table 1 Sensitivity and specificity of clinical examination for diagnosis of synovitis versus MIP images and PD images

Joint	Sensitivity		Specificity	
	MIP	PD	MIP	PD
Wrist	0.52	0.69	1.0	0.89
MCP	0.26	0.57	0.98	0.95
PIP	0.12	–	0.99	–

that predicts subsequent joint damage [3, 28]. The high sensitivity of MIP imaging in the wrist and MCP joints is not surprising because thick palmar ligaments exist in the wrist, and each joint exists side by side in MCP joints. It is striking that the smaller the joints were, the less sensitive clinical findings became, even though PIP joints could be examined from all around the joint.

Contrast-enhanced MRI is an imaging modality for visualization of the inflamed synovium in which there is increased blood flow and increased capillary permeability [13], [29]. A correlation between the thickness of the synovial membrane detected with contrast-enhanced MRI and joint destruction has been reported [5–7]. Several assessments for synovitis have been used, such as rheumatoid arthritis MRI score (RAMRIS), which provides semiquantitative assessments [30–32]; measuring the maximum enhanced thickness of the synovium [6]; and the total volume of the synovial membrane calculated by summation of each slice [7]. All of these methods take time, which makes them difficult to use in busy outpatient settings. Our scoring of synovitis in MIP images is semiquantitative for detecting the volume of the synovial membrane, since the MIP image is a superimposed single 3D image. This scoring is convenient and useful because we can assess simply, using only a single image, and the interobserver agreement is excellent. However, there may be drawbacks with MIP images. Firstly, hyperemia may imitate synovitis, and secondly, the detailed location of the affected anatomical structure is restricted in MIP images. Therefore, we must cross-check MIP images with reference to conventional MR images, although the agreement on synovitis between MIP and conventional MR images was excellent.

US examination is less expensive and more convenient for patients than MRI and can be easily used for repeated examinations. GS and PD images are recorded for the assessment of

Table 2 Number of joints positive and negative on MIP images and PD images

Joint	MIP(+) PD(+)	MIP(+) PD(+)	MIP(−) PD(−)	MIP(−) PD(−)
Wrist	31	16	0	13
MCP	23	61	0	216

MIP(+) positive on MIP image, *MIP(−)* negative on MIP image, *PD(+)* positive on PD image, *PD(−)* negative on PD image

joint inflammation. Synovial hypertrophy is evaluated primarily on GS images, while PD images are utilized to demonstrate activity related to synovial hypertrophy [3, 33, 34]. The clinical significance of GS findings remains disputed [15, 35], and there is also the problem of interobserver agreement [22, 23] (interobserver agreement of GS scores was moderate in this study [data not shown]). The presence of microvascular blood flow in synovial hypertrophy is interpreted as active synovitis and predicts ongoing joint damage even in patients in clinical remission [3, 8, 16, 17, 19, 28, 36, 37]. A high agreement between PD and contrast-enhanced MRI findings of synovitis has been reported [3, 38, 39]. In this study, a statistically significant correlation between MIP and PD findings was shown, and the agreement between grade 2 on MIP images and positive on PD images was substantial for the wrist and moderate for MCP joints. That is, intensive enhancement on MIP images could be a risk factor for further joint damage.

Our results showed that all PD-positive joints were also MIP-positive. We propose two reasons for this result. Firstly, the sensitivity of MIP is so high that it includes inactive synovial membrane thickness. It is not yet clear if there is a level of MRI-detected synovitis below which patients will not show progressive joint destruction [40]. Secondly, the sensitivity of PD is too low. Several factors are known to influence the sensitivity of detecting synovitis by GS and PD. Equipment characteristics and resolution, as well as varying parameter settings, affect sensitivity [34]. Recently, global US scoring systems for synovitis in RA have been challenging to use. Examining a large number of joints takes a considerable amount of time [21, 23, 38]. The minimum number of joints required to evaluate global disease activity is currently being discussed [34]. Also, MRI provides a local, not global, estimation of synovitis; therefore, MRI imaging cannot be used to evaluate global disease activity. One advantage of MRI is that MR images can be reread remotely at a later date; in contrast, US cannot identify abnormalities that are overlooked and not imaged at the time of the original examination. However, increasing use of ultrasound video-loops and 3D ultrasound may assist in this regard in the future [41].

One of the limitations of our study is that the PD images were recorded using a machine widely used in Japan. More sensitive PD signals may be observed using a very high-end machine in the future. In addition to equipment-dependent effects, operator-dependent factors, including factors affecting both image acquisition and interpretation, have to be considered, although all US examinations in our study were performed by a specialist trained in the US examination of rheumatoid hands. Another limitation of this study is that partial enhancement of the joint was graded as grade 1, and complete enhancement of the joint was graded as grade 2, but prospective studies should be conducted to determine the clinical significance of this scoring system. Furthermore, the significance of joints in which PD images are negative and MIP images are positive must be also clarified in a prospective study.

We conclude that using MIP images together with palpation, plain radiographs and conventional MR images allows detailed and comprehensive evaluation of the hand in RA. MIP images may predict ongoing joint damage, since they permit easy semiquantitative evaluation of the degree of thickening of the synovial membrane.

Disclosures None

References

1. Smolen JS, Landewe R, Breedveld FC, Dougados M, Emery P, Gaujoux-Viala C, Gorter S, Knevel R, Nam J, Schoels M, Aletaha D, Buch M, Gossec L, Huizinga T, Bijlsma JW, Burmester G, Combe B, Cutolo M, Gabay C, Gomez-Reino J, Kouloumas M, Kvien TK, Martin-Mola E, McInnes I, Pavelka K, van Riel P, Scholte M, Scott DL, Sokka T, Valesini G, van Vollenhoven R, Winthrop KL, Wong J, Zink A, van der Heijde D (2010) EULAR recommendations for the management of rheumatoid arthritis with synthetic and biological disease-modifying antirheumatic drugs. Ann Rheum Dis 69:964–975
2. Smolen JS, Aletaha D, Bijlsma JW, Breedveld FC, Boumpas D, Burmester G, Combe B, Cutolo M, de Wit M, Dougados M, Emery P, Gibofsky A, Gomez-Reino JJ, Haraoui B, Kalden J, Keystone EC, Kvien TK, McInnes I, Martin-Mola E, Montecucco C, Schoels M, van der Heijde D (2010) Treating rheumatoid arthritis to target: recommendations of an international task force. Ann Rheum Dis 69:631–637
3. Colebatch AN, Edwards CJ, Ostergaard M, van der Heijde D, Balint PV, D'Agostino MA, Forslind K, Grassi W, Haavardsholm EA, Haugeberg G, Jurik AG, Landewe RB, Naredo E, O'Connor PJ, Ostendorf B, Potocki K, Schmidt WA, Smolen JS, Sokolovic S, Watt I, Conaghan PG (2013) EULAR recommendations for the use of imaging of the joints in the clinical management of rheumatoid arthritis. Annals of the rheumatic diseases
4. Suter LG, Fraenkel L, Braithwaite RS (2011) Role of magnetic resonance imaging in the diagnosis and prognosis of rheumatoid arthritis. Arthritis Care Res 63:675–688
5. Boyesen P, Haavardsholm EA, Ostergaard M, van der Heijde D, Sesseng S, Kvien TK (2011) MRI in early rheumatoid arthritis: synovitis and bone marrow oedema are independent predictors of subsequent radiographic progression. Ann Rheum Dis 70:428–433
6. Conaghan PG, O'Connor P, McGonagle D, Astin P, Wakefield RJ, Gibbon WW, Quinn M, Karim Z, Green MJ, Proudman S, Isaacs J, Emery P (2003) Elucidation of the relationship between synovitis and bone damage: a randomized magnetic resonance imaging study of individual joints in patients with early rheumatoid arthritis. Arthritis Rheum 48:64–71
7. Ostergaard M, Hansen M, Stoltenberg M, Gideon P, Klarlund M, Jensen KE, Lorenzen I (1999) Magnetic resonance imaging-determined synovial membrane volume as a marker of disease activity and a predictor of progressive joint destruction in the wrists of patients with rheumatoid arthritis. Arthritis Rheum 42:918–929
8. Brown AK, Conaghan PG, Karim Z, Quinn MA, Ikeda K, Peterfy CG, Hensor E, Wakefield RJ, O'Connor PJ, Emery P (2008) An explanation for the apparent dissociation between clinical remission and continued structural deterioration in rheumatoid arthritis. Arthritis Rheum 58:2958–2967

9. Mori G, Tokunaga D, Takahashi KA, Hojo T, Fujiwara H, Arai Y, Taniguchi D, Takatori R, Imai K, Otakara E, Ito H, Nishimura T, Kubo T (2008) Maximum intensity projection as a tool to diagnose early rheumatoid arthritis. Mod Rheumatol Jpn RheumAssoc 18: 247–251
10. Okumura A, Watanabe Y, Dohke M, Ishimori T, Amoh Y, Oda K, Dodo Y (1999) Contrast-enhanced three-dimensional MR portography. Radiographics: Rev Publ Radiol Soc North Am Inc 19:973–987
11. Aufort S, Charra L, Lesnik A, Bruel JM, Taourel P (2005) Multidetector CT of bowel obstruction: value of post-processing. Eur Radiol 15:2323–2329
12. Ferencik M, Ropers D, Abbara S, Cury RC, Hoffmann U, Nieman K, Brady TJ, Moselewski F, Daniel WG, Achenbach S (2007) Diagnostic accuracy of image postprocessing methods for the detection of coronary artery stenoses by using multidetector CT. Radiology 243:696–702
13. Navalho M, Resende C, Rodrigues AM, Ramos F, Gaspar A, Pereira da Silva JA, Fonseca JE, Campos J, Canhao H (2012) Bilateral MR imaging of the hand and wrist in early and very early inflammatory arthritis: tenosynovitis is associated with progression to rheumatoid arthritis. Radiology 264:823–833
14. Karlo C, Zanetti M, Stolzmann P, Steurer-Dober I, Brunner F, Hodler J, Pfirrmann CW (2011) Synovitis maps for the assessment of inflammatory diseases of the hand. Eur Radiol 21:1499–1508
15. Backhaus M, Kamradt T, Sandrock D, Loreck D, Fritz J, Wolf KJ, Raber H, Hamm B, Burmester GR, Bollow M (1999) Arthritis of the finger joints: a comprehensive approach comparing conventional radiography, scintigraphy, ultrasound, and contrast-enhanced magnetic resonance imaging. Arthritis Rheum 42:1232–1245
16. Naredo E, Collado P, Cruz A, Palop MJ, Cabero F, Richi P, Carmona L, Crespo M (2007) Longitudinal power Doppler ultrasonographic assessment of joint inflammatory activity in early rheumatoid arthritis: predictive value in disease activity and radiologic progression. Arthritis Rheum 57:116–124
17. Scire CA, Montecucco C, Codullo V, Epis O, Todoerti M, Caporali R (2009) Ultrasonographic evaluation of joint involvement in early rheumatoid arthritis in clinical remission: power Doppler signal predicts short-term relapse. Rheumatol (Oxford, England) 48:1092–1097
18. Foltz V, Gandjbakhch F, Etchepare F, Rosenberg C, Tanguy ML, Rozenberg S, Bourgeois P, Fautrel B (2012) Power Doppler ultrasound, but not low-field magnetic resonance imaging, predicts relapse and radiographic disease progression in rheumatoid arthritis patients with low levels of disease activity. Arthritis Rheum 64:67–76
19. Peluso G, Michelutti A, Bosello S, Gremese E, Tolusso B, Ferraccioli G (2011) Clinical and ultrasonographic remission determines different chances of relapse in early and long standing rheumatoid arthritis. Ann Rheum Dis 70:172–175
20. Landis JR, Koch GG (1977) The measurement of observer agreement for categorical data. Biometrics 33:159–174
21. Wakefield RJ, Green MJ, Marzo-Ortega H, Conaghan PG, Gibbon WW, McGonagle D, Proudman S, Emery P (2004) Should oligoarthritis be reclassified? Ultrasound reveals a high prevalence of subclinical disease. Ann Rheum Dis 63:382–385
22. Szkudlarek M, Court-Payen M, Jacobsen S, Klarlund M, Thomsen HS, Ostergaard M (2003) Interobserver agreement in ultrasonography of the finger and toe joints in rheumatoid arthritis. Arthritis Rheum 48:955–962
23. D'Agostino MA, Maillefert JF, Said-Nahal R, Breban M, Ravaud P, Dougados M (2004) Detection of small joint synovitis by ultrasonography: the learning curve of rheumatologists. Ann Rheum Dis 63: 1284–1287
24. Naredo E, Moller I, Moragues C, de Agustin JJ, Scheel AK, Grassi W, de Miguel E, Backhaus M, Balint P, Bruyn GA, D'Agostino MA, Filippucci E, Iagnocco A, Kane D, Koski JM, Mayordomo L, Schmidt WA, Swen WA, Szkudlarek M, Terslev L, Torp-Pedersen S, Uson J, Wakefield RJ, Werner C (2006) Interobserver reliability in musculoskeletal ultrasonography: results from a "Teach the Teachers" rheumatologist course. Ann Rheum Dis 65:14–19
25. Lindegaard H, Vallo J, Horslev-Petersen K, Junker P, Ostergaard M (2001) Low field dedicated magnetic resonance imaging in untreated rheumatoid arthritis of recent onset. Ann Rheum Dis 60:770–776
26. Szkudlarek M, Narvestad E, Klarlund M, Court-Payen M, Thomsen HS, Ostergaard M (2004) Ultrasonography of the metatarsophalangeal joints in rheumatoid arthritis: comparison with magnetic resonance imaging, conventional radiography, and clinical examination. Arthritis Rheum 50:2103–2112
27. Ostendorf B, Scherer A, Modder U, Schneider M (2004) Diagnostic value of magnetic resonance imaging of the forefeet in early rheumatoid arthritis when findings on imaging of the metacarpophalangeal joints of the hands remain normal. Arthritis Rheum 50:2094–2102
28. Brown AK, Quinn MA, Karim Z, Conaghan PG, Peterfy CG, Hensor E, Wakefield RJ, O'Connor PJ, Emery P (2006) Presence of significant synovitis in rheumatoid arthritis patients with disease-modifying antirheumatic drug-induced clinical remission: evidence from an imaging study may explain structural progression. Arthritis Rheum 54:3761–3773
29. Ostendorf B, Peters R, Dann P, Becker A, Scherer A, Wedekind F, Friemann J, Schulitz KP, Modder U, Schneider M (2001) Magnetic resonance imaging and miniarthroscopy of metacarpophalangeal joints: sensitive detection of morphologic changes in rheumatoid arthritis. Arthritis Rheum 44:2492–2502
30. Ostergaard M, Peterfy C, Conaghan P, McQueen F, Bird P, Ejbjerg B, Shnier R, O'Connor P, Klarlund M, Emery P, Genant H, Lassere M, Edmonds J (2003) OMERACT Rheumatoid Arthritis Magnetic Resonance Imaging Studies. Core set of MRI acquisitions, joint pathology definitions, and the OMERACT RA-MRI scoring system. J Rheumatol 30:1385–1386
31. Conaghan P, Bird P, Ejbjerg B, O'Connor P, Peterfy C, McQueen F, Lassere M, Emery P, Shnier R, Edmonds J, Ostergaard M (2005) The EULAR-OMERACT rheumatoid arthritis MRI reference image atlas: the metacarpophalangeal joints. Ann Rheum Dis 64(Suppl 1): i11–i21
32. Ejbjerg B, McQueen F, Lassere M, Haavardsholm E, Conaghan P, O'Connor P, Bird P, Peterfy C, Edmonds J, Szkudlarek M, Genant H, Emery P, Ostergaard M (2005) The EULAR-OMERACT rheumatoid arthritis MRI reference image atlas: the wrist joint. Ann Rheum Dis 64(Suppl 1):i23–i47
33. Walther M, Harms H, Krenn V, Radke S, Faehndrich TP, Gohlke F (2001) Correlation of power Doppler sonography with vascularity of the synovial tissue of the knee joint in patients with osteoarthritis and rheumatoid arthritis. Arthritis Rheum 44:331–338
34. Mandl P, Naredo E, Wakefield RJ, Conaghan PG, D'Agostino MA (2011) A systematic literature review analysis of ultrasound joint count and scoring systems to assess synovitis in rheumatoid arthritis according to the OMERACT filter. J Rheumatol 38:2055–2062
35. Szkudlarek M, Klarlund M, Narvestad E, Court-Payen M, Strandberg C, Jensen KE, Thomsen HS, Ostergaard M (2006) Ultrasonography of the metacarpophalangeal and proximal interphalangeal joints in rheumatoid arthritis: a comparison with magnetic resonance imaging, conventional radiography and clinical examination. Arthritis Res Ther 8:R52
36. Taylor PC, Steuer A, Gruber J, Cosgrove DO, Blomley MJ, Marsters PA, Wagner CL, McClinton C, Maini RN (2004) Comparison of ultrasonographic assessment of synovitis and joint vascularity with radiographic evaluation in a randomized, placebo-controlled study of infliximab therapy in early rheumatoid arthritis. Arthritis Rheum 50: 1107–1116
37. Naredo E, Moller I, Cruz A, Carmona L, Garrido J (2008) Power Doppler ultrasonographic monitoring of response to anti-tumor

necrosis factor therapy in patients with rheumatoid arthritis. Arthritis Rheum 58:2248–2256
38. Terslev L, Torp-Pedersen S, Savnik A, von der Recke P, Qvistgaard E, Danneskiold-Samsoe B, Bliddal H (2003) Doppler ultrasound and magnetic resonance imaging of synovial inflammation of the hand in rheumatoid arthritis: a comparative study. Arthritis Rheum 48:2434–2441
39. Horikoshi M, Suzuki T, Sugihara M, Kondo Y, Tsuboi H, Uehara T, Hama M, Takase K, Ohno S, Ishigatsubo Y, Yoshida Y, Sagawa A, Ikeda K, Ota T, Matsumoto I, Ito S, Sumida T (2010) Comparison of low-field dedicated extremity magnetic resonance imaging with articular ultrasonography in patients with rheumatoid arthritis. Mod Rheumatol Jpn Rheum Assoc 20:556–560
40. Conaghan PG, McQueen FM, Bird P, Peterfy CG, Haavardsholm EA, Gandjbakhch F, Boyesen P, Coates L, Ejbjerg B, Eshed I, Foltz V, Hermann KG, Freeston J, Lillegraven S, Lassere M, Wiell C, Anandarajah A, Duer-Jensen A, O'Connor P, Genant HK, Emery P, Ostergaard M (2011) Update on research and future directions of the OMERACT MRI inflammatory arthritis group. J Rheumatol 38: 2031–2033
41. McNally EG (2008) Ultrasound of the small joints of the hands and feet: current status. Skelet Radiol 37:99–113

Ⅴ．　研究班員名簿

研 究 班 員 名 簿

	氏名	所属研究機関　職名
研究代表者	岡田　正人	聖路加国際大学　聖路加国際病院　アレルギー膠原病科　部長
研究分担者	廣畑　俊成	北里大学医学部　膠原病・感染内科学　教授
	松原　司	松原メイフラワー病院　院長
	萩野　浩	鳥取大学　医学部　保健学科整形外科　教授
	西本　憲弘	東京医科大学　医学総合研究所　難病分子制御学部門　兼任教授
	若林　弘樹	三重大学医学部附属病院　整形外科　講師
	川人　豊	京都府立医科大学　大学院医学研究科　免疫内科学講座　准教授
	岸本　暢将	聖路加国際大学　聖路加国際病院　アレルギー膠原病科　医長
	大出　幸子	聖ルカ・ライフサイエンス研究所　臨床疫学センター　上級研究員
	六反田　諒	聖路加国際大学　聖路加国際病院　アレルギー膠原病科　常勤嘱託医
	土師　陽一郎	宏潤会大同病院　膠原病・リウマチ科　部長
研究協力者	舟橋　恵子	松原メイフラワー病院　臨床研究部　部長
	岸本　勇二	鳥取大学　医学部　運動器医学分野　助教
	村上 美帆	東京医科大学　医学総合研究所　難病分子制御部門　特任助教
	伊藤 眞里	東京医科大学　医学総合研究所　難病分子制御部門　客員講師
	須藤 啓広	三重大学医学部附属病院　整形外科　教授